Accepted Manuscript

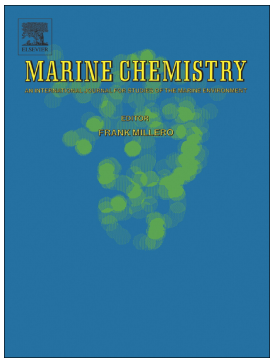

Interactions between iron and organic carbon in a sandy beach subterranean estuary

Maude Sirois, Mathilde Couturier, Andrew Barber, Yves Gélinas, Gwénaëlle Chaillou

PII:	S0304-4203(17)30286-4
DOI:	doi:10.1016/j.marchem.2018.02.004
Reference:	MARCHE 3539
To appear in:	*Marine Chemistry*
Received date:	29 September 2017
Revised date:	23 February 2018
Accepted date:	28 February 2018

Please cite this article as: Maude Sirois, Mathilde Couturier, Andrew Barber, Yves Gélinas, Gwénaëlle Chaillou , Interactions between iron and organic carbon in a sandy beach subterranean estuary. The address for the corresponding author was captured as affiliation for all authors. Please check if appropriate. Marche(2018), doi:10.1016/j.marchem.2018.02.004

Interactions between iron and organic carbon in a sandy beach subterranean estuary

Maude Sirois[1, 2], Mathilde Couturier[1], Andrew Barber[3], Yves Gélinas[3], Gwénaëlle Chaillou[1]

[1]Canadian Research Chair on Geochemistry of Coastal Hydrogeosystems, Québec-Océan, Boreas Group on the North Systems, Université du Québec à Rimouski, 300 Allée des Ursulines, Rimouski, Québec, Canada, G5L 3A1

[2]Institut des Sciences de la Mer de Rimouski, Université du Québec à Rimouski, 310 Allée des Ursulines, Rimouski, Québec, Canada, G5L 3A1

[3]GEOTOP and the Department of Chemistry and Biochemistry, Concordia University, 7141 Sherbrooke St. West, Montréal, Québec, Canada, H4B 1R6

Corresponding author:

Gwénaëlle Chaillou

Université du Québec à Rimouski, 300 Allée des Ursulines, Rimouski, Québec, Canada, G5L 3A1

Gwenaelle_chaillou@uqar.ca

ABSTRACT

Understanding the behavior of terrestrially derived dissolved organic carbon (DOC) through subterranean estuaries (STEs) is essential for determining the carbon budget in coastal waters. However, few studies exist on the interaction of organic carbon (OC) and iron (Fe) in these dynamic systems, where fresh groundwater mixes with recirculated seawater. Here, we focused on the origin and behavior of DOC, and we quantified the relative proportion of OC trapped by reactive Fe-hydroxides along a sandy beach STE. The δ^{13}C-DOC signal in beach groundwater seems to respond rapidly to OC inputs. Our results show a terrestrial imprint from the aquifer matrix dominated by the degradation of particulate organic carbon (POC) issue from an old soil horizon composed of terrestrial plant detritus (^{14}C dating ~800 to 700 years B.P) which is buried below the Holocene sand. Even though the system can be sporadically affected by massive inputs of marine OC, this transient marine imprint seems to be rapidly evacuated from the STE. As reported in soil and in marine mud, Fe–OC trapping occurs in the sandy sediment of the STE. At the groundwater–seawater interface, newly precipitated reactive Fe-hydroxides interact with and trap terrestrial OC independently of the DOC origin in beach groundwater. The molecular fractionation of DOC along the STE and preferential trapping of terrestrial compounds favor the *in situ* degradation and/or export of non-Fe-stabilized marine-derived molecules to coastal waters. These findings support the idea that the sandy beach STE acts as a transient sink for terrestrial OC at the land–sea interface and contributes to the regulation of marine vs. terrestrial carbon exports to coastal waters.

1. Introduction

Sandy beaches are key ecosystems of the global land–sea continuum; they account for more than 70% of the world's ice-free coastline (Emery, 1968; McLachlan and Brown, 2006). While sandy beaches have long been considered as biogeochemical deserts (Huettel et al., 1996), several recent studies have highlighted their importance as biogeochemical reactors where carbon and nutrients are rapidly transformed (Anschutz et al., 2009; Beck et al., 2017; Chaillou et al., 2016, 2014; Charbonnier et al., 2013; Couturier et al., 2017, 2016; Santos et al., 2009, 2008). Their high permeability favors advective transport and the recirculation of seawater, which acts as an important carrier of dissolved carbon species from the coastal ocean into beach groundwater. Moore (1999) proposed the term "subterranean estuary" (STE) for the coastal aquifer zone to emphasize the importance of freshwater and seawater mixing as well as water–particles interactions as water transits toward the sea. As is the case in surface estuaries, the concentration and nature of dissolved species change greatly across the mixing zone of STEs and exhibit both production and removal processes, which often depend on redox conditions. Such processes along the groundwater flow path must be considered when determining accurate chemical fluxes and their impact on the coastal ocean (Beck et al., 2007; Chaillou et al., 2016, 2014; Couturier et al., 2016; Santos et al., 2009).

Most STE studies have focused on nutrients. However, due to the role of the coastal ocean in the global carbon cycle, eutrophication, and ocean acidification, interest has grown in understanding the behavior of both organic and inorganic carbon in STEs. The transport of dissolved organic carbon (DOC) was found to be conservative in some STEs, such as the tidal flats of Hampyeong Bay (South Korea; Kim et al., 2013) and in West Neck Bay (NY, USA; Beck et al., 2007). In contrast, non-conservative DOC behavior was reported during the transit of

groundwater though the mixing zone of STEs, with an apparent production of DOC. This was found in the Gulf of Mexico (USA; Santos et al., 2009), in South Carolina (USA; Goñi and Gardner, 2004) and, more recently, in the Gulf of St. Lawrence (Canada; Chaillou et al., 2016; Couturier et al., 2016). The origin and fate of this DOC pool is still not well described. Marine-derived particles were identified as the main source of carbon in tidal sands (Anschutz et al., 2009; Kim et al., 2012; McLachlan and Brown, 2006). However, Couturier et al. (2016) showed that DOC could also be of terrestrial origin after considering the optical properties of chromophoric dissolved organic matter (CDOM), which showed that lignin- and, more specifically, humic-like dissolved organic matter dominated in the discharge zone. The submarine discharge of terrestrial OC could be a key controlling factor of the optical properties of coastal waters and associated ecosystems (Kim and Kim, 2017).

Several methods have been used to determine the origin of OC in aquatic systems: optical indices of CDOM (Couturier et al., 2016; Kim et al., 2012), lignin oxidation products (Shen et al., 2015), OC fingerprints, and molecular composition by Fourier transform ion cyclotron resonance mass spectrometry (FT-ICR-MS) (Linkhorst et al., 2017; Seidel et al., 2014) as well as the relative contribution of specific amino acids (Shen et al., 2015). OC origin has also been explored by examination of the $\delta^{13}C$ signature of DOC ($\delta^{13}C$-DOC) in soils (Kaiser et al., 2001; Palmer et al., 2011), stream waters (Bouillon et al., 2012; Palmer et al., 2011; Raymond and Bauer, 2001; Sanderman et al., 2009), groundwater from mangrove tidal creeks (Maher et al., 2013), fjords (Yamashita et al., 2015), and estuaries (Barber et al., 2017b; Osburn and Stedmon, 2011). Here, we present the first attempt to discriminate the origin of OC in beach groundwater using the $\delta^{13}C$ signature of DOC. These groundwater samples are particularly challenging to analyze for $\delta^{13}C$

due to the generally low DOC concentrations combined with high salt and, under reducing conditions, with high dissolved iron content.

The difference in the $\delta^{13}C$ signature of marine and terrestrial DOC arises from the initial signature of the carbon source used for its fixation and from the different pathways for carbon fixation during photosynthesis (Guy et al., 1993; Hayes, 1993). Marine DOC is mainly derived from planktonic organisms that use marine dissolved inorganic carbon for carbon fixation during photosynthesis, which has a signature of about 0‰ (Earth System Research Laboratory Global Monitoring Division of NOAA; https://www.esrl.noaa.gov/gmd/dv/iadv/), whereas the ultimate building block for terrestrial DOC is atmospheric CO_2, which has a signature of -8‰ to -9‰ (Earth System Research Laboratory Global Monitoring Division of NOAA; https://www.esrl.noaa.gov/gmd/dv/iadv/). The different photosynthetic fixation pathways used by C3 and C4 plants further induce a biochemical carbon fractionation of about -20‰ (C3) or -12‰ (C4). Combined, the differences in the sources of carbon and in the carbon fixation pathways lead to signatures between about -24‰ and -19‰ for marine primary producers (and marine DOC), between about -28‰ and -25‰ for C3 plant-derived terrestrial DOC, and between about -16‰ to -10‰ for C4 plant-derived DOC (Hedges et al., 1997; Peterson and Fry, 1987; Zeebe and Wolf-Gladrow, 2001).

Iron plays a pivotal role in the chemistry of STEs. The redox oscillations induced by tides, waves, seasonal water table levels, and long-term sea level changes control the precipitation of ferric hydroxides at redox interfaces within the STE (Charette and Sholkovitz, 2002). This Fe curtain acts as an oxidative barrier for redox-sensitive elements and elements with a high affinity for Fe-hydroxides, such as phosphate, barium, uranium, and nitrogen species (Charette et al., 2005; Charette and Sholkovitz, 2006, 2002; Couturier et al., 2017; Sanders et al., 2017). Iron also

interacts with OC and affects its mobility (Kaiser and Guggenberger, 2000) and its molecular properties (Poulin et al., 2014). Predominantly short-term reversible interactions can occur through adsorption, flocculation, or coagulation between Fe-hydroxides and OC, while the direct coprecipitation of Fe and OC, involving covalent bonding between the two elements, can lead to the long-term trapping of carbon under certain redox conditions (Barber et al., 2017a). The molecular composition of OC, and thus its origin, is an important control on the amount of OC trapped in the Fe curtain, along with redox conditions and Fe concentrations. For example, Riedel et al. (2013) showed that aromatic terrestrial OC in peatlands was preferentially trapped compared to aliphatic compounds. Such Fe–OC interactions have been highlighted in marine sediments (Barber et al., 2017a; Keil et al., 1994; Lalonde et al., 2012), soils (Jones and Edwards, 1998; Kaiser and Guggenberger, 2003, 2000; Wagai and Mayer, 2007), and more recently beach groundwater samples (Linkhorst et al., 2017). In this latter study, the authors suggested that Fe induced the flocculation of OC in STEs (mostly large, oxidized, aromatic terrigenous molecules), acting as a potential inorganic regulator for the export of terrestrial OC to coastal waters. This "rusty carbon sink," as proposed by Lalonde et al. (2012), might control not only the submarine groundwater discharge OC fluxes but also the molecular properties of the exported OC (Linkhorst et al., 2017; Seidel et al., 2015, 2014). To our knowledge, there is currently no direct quantification of this carbon sink within STE systems.

In the present work, we focused on the origin and behavior of OC along the STE of a sandy beach located in the Îles-de-la-Madeleine (Gulf of St. Lawrence, QC, Canada), where fresh groundwater flows seaward below a narrow intruding saline circulation cell located near the top of intertidal sediments. We determined both the horizontal and vertical distribution and origin of DOC based on its concentration and stable carbon isotope signature (δ^{13}C-DOC) in beach

groundwater. In addition, we quantified the relative proportion of OC trapped by reactive Fe-hydroxides along a cross-shore transect and determined the isotopic signature of the Fe-stabilized OC.

2. Materials and Methods

2.1 Site Description

This study was conducted in the STE of Martinique Beach in the Îles-de-la-Madeleine (Québec, Canada) (Fig. 1). This archipelago is located in the Maritimes Permo-carboniferous Shelf Basin (Brisebois, 1981). The main aquifer of the archipelago is composed of sandstones from the Permian Inferior period (the Cap-aux-Meules formation; Brisebois, 1981) with a mean transmissivity of 1.5–4×10^3 m^2/s and a mean recharge of 230 mm/y (i.e., 25–30% of the annual precipitation; Madelin'Eau, 2004). Like other aquifers in this region, the groundwater recharge is mainly controlled by the snow-pack melt in May and early June that rapidly influences the water table levels. Groundwater flows through this unconfined aquifer and discharges into the ocean through the overlying permeable tidal deposits with a mean annual flow of 0.020 m^3/s (Madelin' Eau, 2004). The submarine groundwater discharge is higher in June, with a total flow of around 0.040 m^3/s near the shoreline, more than 50% of which is composed of fresh and meteoric groundwater (Chaillou et al., 2017).

In the Gulf of Saint Lawrence, the Îles-de-la-Madeleine currently experience rates of relative sea-level rise that are higher than the global average, ranging between 1.3 and 2.0 mm for the past 2000 years (Barnett et al., 2017). This rapid rise buried the unconfined Permian sandstone aquifer, which is now covered by tidal sediment (Barnett et al., 2017). Tidal sediment consists of a ~50 cm thick layer of eolian sand with an average grain size of ~300 µm that is mainly

composed of quartz (95%) mixed with silt (<5%; Chaillou et al., 2014) and has a mean hydraulic conductivity of 11.4×10^3 cm/d. The underlying Permian sandstone aquifer consists of fine red-orange sands (~100 µm) composed of silicate and aluminosilicate with Fe oxides coating silicate grains (Chaillou et al., 2014); the mean hydraulic conductivity is 4.8×10^3 cm/d. Its exact localization in the beach and its offshore extent are unknown. At the top of the sandstone aquifer, there is a fragmented organic-rich layer, mainly composed of terrestrial plant detritus formed ~800 to 700 years B.P., as revealed by ^{14}C dating of lignose fragments and conifer needles (Barnett et al., 2017). The site experiences little wave action except during storm events, preventing the complete erosion of this layer. Tides are semi-diurnal with a spring tide range $\leq$1 m.

A few recent studies have focused on the biogeochemistry of the STE (Couturier et al., 2017, 2016) and the calculation of groundwater flows (Chaillou et al. 2018, 2016) at the Martinique Beach site. The shallow superficial unconfined beach aquifer releases both fresh groundwater and recirculated seawater to the coastal embayment. Within the beach, fresh groundwater flows towards the seaward discharge region at a mean velocity of 0.30 m/d and discharges below a narrow upper saline plume (USP) located near the top of the intertidal sediments. This fresh groundwater contributes at least 50% of the total water flow discharging to the coastal waters. Based on mean DOC concentrations in the surficial intertidal sediment, Chaillou et al. (2016) calculated a fresh-groundwater carbon load of 27 kg/d of DOC at the discharge zone. They concluded that fresh groundwater was not the source of carbon in the STE, but it was a pathway for DOC produced in the beach to reach the coastal ocean. Based on optical indices of CDOM, Couturier et al. (2016) recently showed that the degradation of the old buried soil is a probable source of the OC pool in beach groundwater. This degradation during the transit modified the

optical fingerprint of groundwater OC by releasing high molecular weight (HMW), aromatic, lignin-type compounds of terrestrial origin (Xie et al., this special issue).

2.2 Beach groundwater sampling

Samples were collected during the neap tide period in May and June of both 2013 and 2015. Water samples were collected using nine multi-level samplers inserted along a ~20 m transect perpendicular to the shoreline (Fig. 2A). The positions of the multi-level samplers covered the intertidal zone and the underlying STE, where fresh groundwater comes in contact with recirculated seawater. In 2013, multi-level samplers M2, M4, M5, M6, M7, and M8 were used to collect beach groundwater. In 2015, groundwater samples were collected twice following a storm that left seaweed on the beach, using multi-level samplers M1, M3, M6, and M9. The samples were collected one and three days after the massive deposition of seaweed fragments (Fig. 2D), which were mainly composed of *Zostera marina*.

Each multi-level sampler allowed the collection of beach groundwater at eight depths (~10, 30, 50, 80, 110, 150, 190, and 230 cm) below the beach surface. To allow sediments around the samplers to reach equilibrium, multi-level samplers were installed for a minimum of two days prior to beach groundwater collection. During collection, groundwater was continuously pumped to the surface using a peristaltic pump and Tygon tube. Salinity, temperature, and dissolved oxygen were measured in an in-line flow cell with a calibrated YSI-600QS multiparametric probe. After stabilization of these parameters, beach groundwater samples were collected with a clean polypropylene syringe and filtered through combusted 0.7 µm glass fiber filters. Samples were acidified to pH<2 with pure HCl in EPA borosilicate vials with PTFE lined caps for subsequent DOC and δ^{13}C-DOC analyses. For total dissolved Fe, beach groundwater samples

were filtered through 0.2 µm Whatman Polycap 75S filters and acidified with pure nitric acid to pH<2 in polypropylene Falcon® tubes. Samples were stored at 4°C.

Concentrations of DOC and Fe as well as the δ^{13}C-DOC signatures were systematically measured for the fresh inland groundwater and seawater end-members. Samples from the Permian sandstone aquifer were pumped from a municipal well located 1.5 km from the shore (PU6; Fig. 1C), and one private well (PC; Fig. 1C) located ~50 m inshore from the multi-level sampler transect. Marine end-members were collected from 0 to 0.6 km offshore in Martinique Bay using a small boat from which seawater was collected using a submersible pump connected to an on-line flow cell. Physico-chemical parameters were measured and samples for DOC, total dissolved Fe, and δ^{13}C-DOC were collected and stored as described above.

2.3 Beach sediment sampling

Three sediment cores were collected in 2013 using standard vibracoring techniques with a clean plastic 1 m liner inserted into an aluminum pipe. The cores were recovered at the top of the beach (C1; Fig. 2B) and at the high- and low-tide marks (C3 and C4; Fig. 2B). The cores were frozen at -20°C until subsampling. Cores were then opened and the three different sedimentary units (i.e., Holocene sand, organic-rich horizon, and Permian sandstone) were subsampled to measure their particulate organic carbon (POC) concentration, isotopic signature (δ^{13}C-POC), reactive Fe-hydroxide content, and the concentration and stable isotope signature of POC, which is trapped on Fe-hydroxides. In 2015, the three different sedimentary units (i.e., Holocene sands, Permian sandstone, and the organic-rich horizon) were collected in the intertidal zone with a manual auger at the high- and low-tide marks (C2 and C5; Fig. 2B). The samples were frozen at -20°C until subsequent analysis. Because they can act as a potential source of DOC to the beach

system, seaweed that accumulated at the surface of the intertidal zone in 2015 was also collected to measure the POC concentration and stable isotope signature (δ^{13}C-POC). Three replicate samples were collected and frozen at -20°C prior to subsequent analysis.

2.4 Chemical Analyses

2.4.1 Dissolved Compounds

Total dissolved Fe concentrations were analyzed in acidified and filtered samples using a Microwave Plasma Atomic Emission Spectrophotometer (4200 MP-AES; Agilent Technologies). The detection limit of the method is 2.4 µg/L for Fe concentration at a wavelength of 391 nm; analytical uncertainties were <5%.

For the samples collected in 2013, DOC was analyzed by high temperature combustion (HTC) using a total organic carbon (TOC) analyzer (TOC-V_{cpn}; Shimadzu) based on the method proposed by Wurl and Tsai (2009) (see Couturier et al., 2016, for details). The detection limit is 0.05 mg/L and analytical uncertainties were <2% for concentrations higher than 1 mg/L. Samples for DOC concentrations in 2015 and δ^{13}C-DOC in 2013 and 2015 were analyzed using a modified Aurora OI 1030 high-temperature catalytic oxidation unit coupled to a chemical trap (GD-100; Graden Instruments) and a GV Isotope Ratio Mass Spectrometer (Isoprime) as described in detail in Lalonde et al. (2014a) and Barber et al. (2017b). The standards used for isotopic signatures and DOC concentrations were in-house calibrated β-alanine (40.4% OC, -26.1 ± 0.1‰) and sucrose (42.1% OC, -11.8±0.1‰) dissolved in 18.2 mΩ/cm milli-Q water (Barber et al., 2017b). The precision of the method for fresh and salt waters is ±0.5‰ for DOC

concentrations of 0.5 mg/L, decreasing regularly from ±0.5‰ to ±0.2‰ between 0.5 and 1.0 mg/L, and ±0.2‰ above 1.0 mg/L (Lalonde et al., 2014a).

2.4.2 Particulate fraction

The citrate-dithionite-bicarbonate Fe reduction method of Mehra and Jackson (1960) modified by Lalonde et al. (2012) was applied to the dried and homogenized sediments. This method allows quantification of the fraction of total POC that is specifically associated with reactive Fe-hydroxides as well as its $\delta^{13}C$ signature. Briefly, reactive Fe-hydroxides are reductively dissolved with dithionite at circumneutral pH (bicarbonate buffer) using citrate as a complexing agent to keep dissolved Fe in solution. The fraction of OC associated with reactive Fe-hydroxides was measured by the difference before and after the reduction reaction. The OC concentration and carbon stable isotope signature were analyzed with an elemental analyzer (Eurovector EuroEA3000) coupled to a GV Instrument Isoprime isotope ratio mass spectrometer following the removal of inorganic carbon by vapor-phase acidification (Hedges and Stern, 1984). The reactive Fe-hydroxide content in the extract following the reduction step was analyzed by inductively coupled plasma mass spectrometry (Agilent 7500ce). The sedimentary units in each core were analyzed in triplicate in 2013 and 2015. The analytical precision was better than ±0.2% for organic carbon concentrations and ±0.2‰ for the stable carbon isotope signatures.

3. Results

3.1 Characteristics of the potential dissolved organic carbon sources

The characteristics of the different potential sources of DOC are presented in Table 1. The fresh inland groundwater samples exhibited DOC concentrations and $\delta^{13}C$-DOC signatures

ranging from 0.4±0.1 to 2.3±0.4 mM and -26.0±1.1‰ to -20.6±6.2‰, respectively. The highest DOC concentrations were measured in the private well PC, located close to the shore. Its δ^{13}C-DOC signature was very depleted. Seawater exhibited low DOC concentrations around 0.15 mM with a mean δ^{13}C signature of -22.2 ± 4.3‰, which is typical of marine signatures (Peterson and Fry, 1987) and in the range of values recently reported for water samples collected in the Gulf of St. Lawrence (Barber et al., 2017b). Our seawater values are, however, slightly depleted compared to the most enriched values of -20.3 ± 0.7‰ that Barber and co-authors (2017) proposed as an "appropriate" marine end-member for the St. Lawrence Estuary and Gulf region.

3.2 Biogeochemical features of the STE

Recent studies have focused on the variations of physio-chemical parameters (salinity, temperature, pH, dissolved oxygen) and DOC concentrations along the groundwater flow path from inland wells to Martinique Beach and the adjacent bay (see Couturier et al., 2017, and references therein). Here, we briefly present the spatial distribution of salinity, Fe, and DOC concentrations in May and June 2013 and 2015.

The spatial distribution of salinity along the transect was relatively similar in 2013 and 2015, with an upper recirculation seawater cell just below the beach surface where salinity was higher than 20 (Fig. 3A-C). In 2013, this zone was vertically constrained with a maximum extension to a depth of 0.5 m. In 2015 (Fig. 3B-C), however, seawater infiltration was deeper, reaching a depth of 1 m below the beach surface. Brackish water, with salinities ranging from 2 to 20, formed a thin mixing zone along the perimeter of the upper recirculation cell. The deeper part of the STE was dominated by seaward-flowing fresh groundwater with low salinity (<2).

The vertical and horizontal distribution of salinity along the transect agreed well with the concept of a subterranean estuary proposed by Moore (1999).

Dissolved Fe exhibited strong vertical gradients, with lower concentrations at the surface to concentrations higher than 1000 µM in brackish groundwater. In 2013, Fe concentrations in beach groundwater were very high, with a mean value around 600 µM. Dissolved Fe increased just below the upper seawater recirculation cell and reached values higher than 500 µM in the mixing zone (Fig. 3D). In the deep groundwater, concentrations remained high (range: 500 to 1500 µM) and reached values as high as 2300 µM in M4. In 2015, the patterns of Fe concentrations were different (Fig. 3E-F). Since the upper recirculation cell was deeper, the dissolved Fe-rich zone was located just below the surface at the low-tide mark (from M6 to M9; Fig. 3E-F). The concentrations were also lower, with mean values around 400 µM and maxima below 1800 µM.

In beach groundwater, DOC concentrations ranged from 0.14 to 15.28 mM, well above the concentrations measured in the water end-members (Table 1). The distribution patterns were all characterized by low concentrations (<2 mM) in the intertidal zone, from M5 to M7. The DOC-enriched zone was located at the high-tide mark near M3 and M4. However, mean concentrations were significantly different in the three sampling periods. In 2013, DOC concentrations ranged between 0.14 and 15.28 mM with a mean value of 2.10±2.63 mM. The highest concentrations (>10 mM) were measured at about 80 cm depth below the surface in M4 (Fig. 3D). In 2015-A, the DOC concentrations ranged from 1.18±0.04 mM to 12.41±0.22 mM with a slightly higher mean value of 3.30±2.17 mM. The highest concentration occurred at the interface between seawater and sediment between M3 and M6 (Fig. 3H). Two days later, the mean DOC concentration decreased to 2.72±3.18 mM (from 0.63±0.05 mM to 13.62±0.12 mM).

The DOC concentration was higher than 12 mM at the top of the intertidal zone, near the surface of M3 (Fig. 3I).

The $\delta^{13}C$ signatures of DOC were very different between 2013 and 2015. In 2013, the $\delta^{13}C$-DOC signatures were between -31.2±0.1‰ and -22.7±0.1‰, with a mean value of -26.4±1.6‰. Values were generally close to -25‰, but they were more depleted in ^{13}C at the high-tide mark, where they dropped to about -30‰. These values corresponded to a terrestrial $\delta^{13}C$ signature. In 2015-A, just one day after the massive seaweed deposit, values were less depleted in ^{13}C compared to 2013, with signatures between -23.7±0.1‰ and -12.4±0.1‰ (mean of -16.1±3.0‰). The isotopic enrichment was very clear in the intertidal zone, between M6 and M9, where signatures were between -17.0±0.2‰ and -12.4±0.1‰. Three days later (2015-B), the $\delta^{13}C$-DOC signatures were still enriched in ^{13}C compared to 2013 (between -25.3±0.2‰ and -12.2±0.02‰; mean = -19.0±3.3‰), but not as much as in 2015-A. The $\delta^{13}C$-DOC signatures were enriched in ^{13}C between 50 and 80 cm in depth in the intertidal zone (between -12.2±0.1‰ and -16.9±0.2‰) compared to the samples located above the high-tide mark, where $\delta^{13}C$ was around -20‰.

3.3 Source, Distribution, and Signature of POC along the transect

The four other investigated sources of OC correspond to solid phase terrestrial and marine organic matter. The Holocene sand and Permian sandstone matrix were poor in OC, with concentrations below 0.5% in dry sediment (Fig 4). In both cases, the $\delta^{13}C$-POC signatures were depleted and ranged between -25.20±1.60‰ (n=17) and -26.50±0.10‰ (n=15) in the sands and sandstone, respectively. Two organic-rich source materials were also present in the system,

namely, the old soil buried below the Holocene sand and the fresh seaweed deposit at the top of the Holocene sand in the intertidal zone. The particulate organic carbon (POC) content in the old buried soil was high at the top of the beach, with POC content >19.6% (Fig. 4). This content tended to decrease towards the shoreline, where this horizon was eroded away or degraded. This layer was detected only in core C2 in 2015, although it was more diluted with minerals at this site than in 2013 (OC content of about 5%). In all cases, this POC exhibited a δ^{13}C signature typical of terrestrial soil (i.e., -26.70±0.50‰; n=9). The marine seaweeds collected on the beach were enriched in POC (30.30±0.80%). However, this sporadic deposit was characterized by a enriched δ^{13}C-POC signature (i.e., -12.00±0.20‰; n=3) typical of *Zostera marina* (Chmura and Aharon, 1995).

3.4 Distribution and Signature of the Organic Carbon Trapped by Fe-oxides along the STE

The relative amounts of OC associated with reactive Fe-hydroxides in the different sedimentary units are reported in Figure 5. The percentage of total OC associated with reactive Fe-hydroxides was low in the 2013 samples, with values below 13.9% in the three units. In the seaward core (C4), where the total OC concentrations were very low (<1 wt%), the proportion of OC associated with reactive Fe-oxides was below the method's detection limit. Higher percentages of total OC associated with Fe were measured in sediment samples collected in 2015, particularly for core C2, where Fe-stabilized OC accounted for about 24% in the surficial sand unit and increased with depth to reach a maximum value of 56% in the Permian sandstone (Fig. 5). The δ^{13}C-POC signature of the OC associated with reactive Fe was very depleted and ranged between -24.30 and -33.60‰.

4. Discussion

4.1 Biogeochemical process along the STE

The STE of Martinique Beach is a highly dynamic system characterized by transient biogeochemical conditions where dissolved oxygen saturation, DOC, and Fe concentrations vary greatly within centimeter-scales. As in surficial estuaries, different processes, such as mineralization, flocculation, adsorption, and coprecipitation, can affect the fate of DOC and Fe in beach groundwater. The absence of light and continuous water–sediment interactions provide an ideal environment for the transformation and sorption of OC onto mineral particles in the absence of photochemical oxidation processes (Kaiser et al., 2004). In addition, the mineralization of OC leads to a decrease in DOC concentrations and the production of DIC and reduced metabolites such as dissolved ferrous iron (Bauer et al., 2013; Dorsett et al., 2011; Nevin and Lovley, 2002; Roy et al., 2013). As in surficial estuaries, the salinity gradient also induces the flocculation of OC and the formation of Fe colloids (Boyle et al., 1977; Charette and Sholkovitz, 2002; Haese, 2006).

In the sandy beach STE, DOC clearly showed a non-conservative pattern, with significant internal inputs during the transit of groundwater along the intertidal zone (Fig. 3G-I). This is similar to what has already been observed at the same site (Chaillou et al., 2016; Couturier et al., 2016) and in other STEs, including Turkey Point Beach (Gulf of Mexico, Florida; Santos et al., 2009), Hampyeong Bay (Korea; Kim et al., 2012), and North Inlet (South Carolina; Goñi and Gardner, 2004). The low dissolved oxygen saturation (~20%) and high DOC concentrations (>2 mM) suggest that the environment is suitable for anaerobic microbial respiration. The high DIC concentrations previously reported by Chaillou et al. (2014, 2016) combined with high dissolved Fe concentrations (and other reduced compounds such as NH_4^+ and Mn^{2+}; Couturier et

al., 2017) as well as the characteristic H_2S odor detected during sample collection all support the idea that suboxic to anoxic OC mineralization processes occurred along the flow path, supporting the loss of both POC and DOC towards the discharge zone.

The spatial distributions of dissolved Fe also showed a non-conservative pattern and a significant difference between the high Fe concentrations in the deep part of the STE, where fresh groundwater flowed in 2013 (Fig. 3D), and the low-tide mark of the upper saline plume (USP) in 2015, where seawater recirculated (Fig. 3F). The accumulation and degradation of the fresh seaweed deposit likely increased OC mineralization rates and, therefore, enhanced the consumption of oxidants and the production of reduced chemicals near the beach surface. This finding agrees well with the high NH_4^+ concentrations observed by Couturier et al. (2017) in the USP. The redox oscillation within the mixing zone along the USP creates favorable conditions for Fe–OC flocculation and oxidative precipitation mechanisms because oxidation of ferrous Fe from anoxic groundwater is efficient near the groundwater–seawater interface, where dissolved oxygen levels and salinity increase due to tidal inputs (Charette and Sholkovitz, 2002; Edzwald et al., 1974; Sholkovitz, 1976). The low mean concentrations of dissolved Fe in beach groundwater in 2015 suggest a general loss of dissolved Fe to the solid phase compared to 2013. The oxidation and precipitation of reactive Fe-hydroxides were probably more efficient during this sampling period. Because the Fe-hydroxide content of the solid phase is very high in both the Holocene sand and the underlying Permian sandstone aquifer, the direct measurement of newly formed amorphous Fe-hydroxides was not possible using this extraction method. In addition to reactive Fe-hydroxide precipitation, Riedel et al. (2013) reported that the oxic–anoxic transition enhances the mechanism of Fe–OC flocculation, particularly with terrestrial OC, controlling the export of both Fe and lignin-type compounds to the overlying water column.

4.2 Source of the DOC in the study beach based on δ^{13}C-DOC signatures

Based on the stable isotopes of water along the STE, Chaillou et al. (2018) confirmed the contribution of only two water end-members (i.e., fresh inland groundwater mainly originated from snow melt and seawater) and the absence of additional septic tank seepages, which could act as a source of OC into beach groundwater. The surficial runoff cannot be totally excluded. However, the absence of important rain events during the days prior to the sampling period and the high level of the water table limit the infiltration of surficial drainage enriched in terrestrial OC within the system. Chaillou et al. (2018) also highlighted the high contribution of fresh inland groundwater and the limited infiltration of seawater in shallow beach groundwater in spring, when the water table is high due to the snowmelt.

In contrast to the spatial distribution of DOC, the δ^{13}C-DOC signatures exhibited different values and patterns in 2013 and 2015. Even though the DOC concentrations were in the same range (Fig. 3G-I; Fig. 6), the average isotopic signatures varied greatly, from -31.2±0.1‰ in 2013 to -12.2±0.1‰ in 2015-A, when seaweeds were deposited on the beach. In both cases, the groundwater end-members did not seem to be the primary source of DOC in beach groundwater because their respective signatures (i.e., -14.4±0.1‰, -20.6±6.2‰, and -22.1±4.3‰ for fresh inland groundwater of P4 and PU6 and for seawater, respectively; Table 1) were very different from the beach groundwater DOC signatures. Even if there was limited infiltration of seawater below the USP, we cannot exclude the possibility that some DOC derived from marine primary production was present in the system. However, it was clearly not the main source of DOC. This suggests that the beach groundwater DOC pool was disconnected from the water end-members. With a maximum groundwater flow rate of ~0.30 m/d within the beach aquifer (Chaillou et al.,

2016), the groundwater transit time through the STE (~20 m) is about 66 days, which is long enough to allow DOC production from the degradation of POC from both marine and terrestrial origins. In addition, other processes can influence the measured δ^{13}C-DOC signatures, such as the degradation of DOC and the biochemical fractionation of the dissolved organic compounds based on their size and affinity for the mineral phase. As an example, DOC production rates from seaweed degradation are highest in the first 1–2 days and decrease afterward (Wada et al., 2007, and reference therein).

In the 2013 samples, the beach groundwater δ^{13}C-DOC signatures ranged from -31.2±0.1‰ to -22.7±0.1‰ (Fig. 3J-L, Fig. 6) and were typical of terrestrial plants that use the Rubisco enzyme in C fixation during photosynthesis (C_3 plants). These signatures were strongly depleted compared to the values measured in the fresh inland groundwater samples with the exception of the nearshore well (PC), where the δ^{13}C-DOC signature was -26.0±1.1‰ (Table 1). The variations in δ^{13}C-DOC signatures along the flow path from the aquifer to the beach groundwater reflect the land cover and soil, which are the main sources of DOC to fresh groundwater (Shen et al., 2015, and references therein). The unsaturated zone acts as a chromatographic column, where surface and plant-derived DOC are removed by microbial degradation and sorption onto minerals prior to reaching the saturated zone (Shen et al., 2015). The proximity of the PC well to the studied transect and the thickness and lithology of the unsaturated zone probably prevent the extensive removal of surficial and plant-derived DOC. In PC well, significantly higher $SUVA_{254}$ values (i.e., DOC-normalized absorbance at 254 nm; Weishaar et al., 2003) were measured compared to values measured in municipal wells, corroborating the relatively high concentrations of plant-derived CDOM in beach groundwater (Couturier et al., 2016; Xie et al., this special edition). The δ^{13}C-DOC signatures were close to

$\delta^{13}C$ values of POC from the old buried soil and sediments, which exhibited signatures typical of terrestrial C3 plants (Aravena et al., 2004; Aravena and Wassenaar, 1993; Palmer et al., 2011). This result suggests that the degradation of this terrestrial POC supported the production of DOC, in agreement with the findings of Couturier et al. (2016). This process probably supported both the production of DIC with a depleted isotopic signature (e.g., about -30‰; Chaillou et al., 2016) and the release of DOC, probably as aromatic lignin-type compounds, in agreement with the findings of Filip and Smed-Hildmann (1992), who showed that fossil plant materials could release humic acids to groundwater.

The DOC concentrations and $\delta^{13}C$-DOC signatures measured in the 2015 beach groundwater samples were significantly different from those measured in 2013. During the first sampling campaign in 2015 (2015-A), which was only one day following the massive deposition of seaweed on the beach, we measured $\delta^{13}C$-DOC signatures ranging between -23.7±0.1 and -12.4±0.1‰ (Fig. 3K), which were less depleted compared to 2013 (Fig. 3J). As in 2013, the degradation of a specific POC source material might control the isotopic signatures of DOC in the beach groundwater samples. The massive seaweed deposit represented a source of organic material with an OC content of 30.3±0.8% (wt) and a stable isotope signature of -12.0±0.2‰, similar to some of the $\delta^{13}C$-DOC signatures measured in 2015-A. Seaweed deposits, which accumulate sporadically along the shore during storm events, may fuel the *in situ* release of DOC with a C4 plant signature. This release of DOC determines the stable isotopic signature of DOC near the surface of the beach for as long as the seaweed deposit is present at the surface. Only three days after the deposit event, however, the isotopic imprint of seaweed was diluted and $\delta^{13}C$-DOC signatures reached more depleted values (Fig. 6). The DOC originating from seaweed degradation is likely rapidly flushed through the discharge zone by both the tidal pump and the

hydraulic head gradient. Based on the specific groundwater discharge measured in this site, we calculated that around 8000 m^3 of beach groundwater were exported from the intertidal zone in only three days. The seaweed-derived DOC was probably transported by submarine groundwater discharge to coastal water, and the isotopic signature was probably diluted by more depleted $\delta^{13}C$ signatures derived from the buried soil and aquifer matrix.

The $\delta^{13}C$-DOC signal in beach groundwater seems to rapidly respond to OC inputs. We observed a terrestrial imprint from the aquifer matrix resulting from the POC degradation from the old buried soil and sediment. However, the system can be sporadically affected by massive inputs of marine OC, which masks the terrestrial imprint. This transient marine imprint seems to be rapidly evacuated from the STE. The stable isotope signature of the DOC pool is likely an efficient tracer of these rapid changes in source material in the sandy beach STE.

4.3 Fe–OC interactions along the STE

Mineralogy, and more specifically mineral surface chemistry and area, largely controls the stabilization of OM in soils (Kaiser and Guggenberger, 2003) and sediment (Hedges and Keil, 1995). In a broad range of cohesive marine sediments, for example, Lalonde et al. (2012) showed that on average 21.5±8.6% of total OC was closely associated with, or trapped by, reactive Fe-hydroxides through adsorption onto and/or coprecipitation with reactive Fe-hydroxide. In the non-cohesive sediments of the STE, the average grain size decreases with depth, from ~300 µm in surficial Holocene sand to ~100 µm in Permian sandstone. Surprisingly, this decreasing trend is not paralleled by an increase in reactive Fe-hydroxide concentrations, which vary between about 1 and 6% of the total sediment dry weight, with slightly higher concentrations in 2015-A and 2015-B compared to 2013 (Table S1). The amounts of OC associated with Fe (percent of

total OC) shown in Figure 5 are thus not controlled by the amount of available reactive Fe-hydroxides; this is as also suggested by the very low OC:Fe molar ratios (<2.07; Table S1) calculated for both years. While the total OC concentrations in the organic-poor layers (Holocene sand and Permian sandstone) were low in both years, a higher fraction of this OC was stabilized through its association with reactive Fe-hydroxides in 2015 (5.8 to 56.3% of total OC) compared to 2013 (non-detectable to 13.9% of total OC), with a maximum in the high-tide mark core C2 (Fig. 5). We know that the difference was not directly due to the generally higher, seaweed-derived DOC concentrations measured in 2015 close to the beach surface (Fig. 3G-I) because the $\delta^{13}C$ signature of Fe-associated OC was typical of soils (about -27‰) rather than seaweeds (about -12‰). The absence of a seaweed signal in the Fe-associated POC fraction could be due to the fact that this large input of fresh seaweed-derived DOC enhanced microbial activity, which in turn resulted in mildly reducing conditions, thus limiting the trapping of this fresh material onto the solid phase. The resulting displacement of the oxic–anoxic transition zone then led to an enhancement in Fe–OC trapping when reducing groundwater enriched in dissolved ferrous iron was oxidized and dissolved Fe re-precipitated as reactive Fe-hydroxides in contact with oxygenated seawater. These newly precipitated reactive Fe-hydroxides probably acted as a "transient" barrier to the DOC pool, which has the highest affinity with amorphous reactive Fe-oxides (Gregory and Duan, 2001; Linkhorst et al., 2017). The concomitant presence of reduced Fe and DOC under anaerobic conditions and the subsequent precipitation of Fe–OC at the oxic–anoxic transition zone support the idea of the highly dynamic nature of such an Fe curtain in response to fresh organic matter inputs.

The increase with depth in the relative proportion of total OC associated with reactive Fe-hydroxides measured in both years (Fig. 5) could be due in part to the downward increase in

particle surface area, although the mineral grains in the three sedimentary units all belonged to the sandstone category (i.e., large particle size, low mineral surface reactivity). Other factors such as the local redox conditions, the bacterial degradation of non-Fe-stabilized OC, the molecular composition of the Fe-stabilized OC, and others remaining to be identified, could have played a role. We should emphasize that the challenge associated with the sampling of pore water corresponding exactly to the analyzed solid phase samples in non-cohesive sediments such as a sandy beach, the fact that the cores were not all sampled during the same year, and the highly dynamic nature of STE make the interpretation of the data extremely difficult. More work is needed to fully understand the mechanism(s) and types of chemical bonds that lead to the trapping of terrestrial OC through adsorption onto and/or coprecipitation within reactive Fe-oxides in this system.

The interactions between Fe and DOC are modulated by local redox conditions and by the molecular composition and concentrations of OC (Riedel et al., 2013; Sholkovitz, 1976). The measured δ^{13}C-POC signatures shown in Figure 5 indicate that the Fe-associated POC pool is of terrestrial origin regardless the sedimentary unit. Reactive Fe-oxides have a greater affinity for high molecular weight compounds enriched in aromatic, carboxylic, and hydroxyl moieties, such as altered lignin and polysaccharide compounds of terrestrial origin, compared to the more aliphatic-rich compounds characteristic of marine OC (Linkhorst et al., 2017; Riedel et al., 2012; Shields et al., 2016). Ferric iron in STE groundwater preferentially interacts with and traps terrestrial OC independently of the origin of the DOC in beach groundwater. The molecular fractionation of DOC along the STE and preferential trapping of terrestrial compounds favor the *in situ* degradation and/or export of non-Fe-stabilized marine-derived molecules to coastal waters. This, along with the preferential photodegradation of aromatic-rich compounds (Lalonde

et al., 2014b), explains in part the globally low concentrations of humic-like DOM observed in coastal embayments (Kim and Kim, 2017). The exact mechanism controlling these Fe–OC interactions (i.e., adsorption or coprecipitation of OC on a mineral surface; Barber et al., 2017a) remains to be determined, and further laboratory experiments are required to explore the role of the Fe curtain as a permanent or transient terrestrial carbon sink at the groundwater–seawater interface. As recently suggested by Shields et al. (2016), this trapped iron-associated OC can also form the basement to support the accumulation of even more OC as the beach system evolves. In agreement with the idea of Linkhorst et al. (2017), however, we propose that STEs act as transient sinks for terrestrial OC at the land–sea interface and contribute to the regulation of marine vs. terrestrial carbon exports to coastal waters. This inorganic regulator may contribute to the "missing" terrestrial OC in the ocean (Bianchi, 2011; Hedges et al., 1997).

5. Conclusion

The analysis of $\delta^{13}C$ signatures of DOC allowed the discrimination of its sources in the studied STE. The OC sources appeared partly decoupled from the water masses of STE. The first source is terrestrial and originates in large part from an old buried soil present in the aquifer matrix that releases ^{13}C-depleted DOC as it is degraded. This DOC constitutes the baseline signal in the beach aquifer. The other major source of DOC detected in this system is rapidly degrading seaweed that sporadically accumulates on the beach surface in response to storm events. The intensity of this transient signal can be so high that it can mask the baseline $\delta^{13}C$-DOC signal, as was the case in this study in 2015. These results further confirm that a high-frequency sampling approach should be adopted to adequately decipher the cycling of OC in systems as dynamic as this one since individual sampling efforts are only a snapshot of the OC pools and fluxes.

Our study highlights that Fe–OC trapping occurs in the non-cohesive sediment of a sandy beach STE. Newly precipitated reactive Fe-hydroxides probably play a pivotal role as a transient barrier to the DOC pool, more specifically on terrestrial-derived organic carbon. As in soil and in cohesive marine sediments, the molecular fractionation of DOC along the STE and the preferential trapping of terrestrial compounds favor the *in situ* degradation and/or export of non-Fe-stabilized marine-derived molecules to coastal waters. These mechanisms contribute to the regulation of marine vs. terrestrial carbon exports to coastal waters. The exact role of the Fe curtain as a permanent or transient terrestrial carbon sink at the groundwater–seawater interface remains to be determined and should be explored in future studies. Whether on a transient or long-term basis, this trapped iron-associated OC can also form a seeding template that eventually leads to the accumulation of even more OC as the beach system evolves. Within the context of climate change and the inevitable sea-level rise, the impact of buried terrestrial horizons on carbon fluxes needs to be understood in order to assess the consequences of the landward migration of the coastline on the biogeochemistry of coastal oceans.

Acknowledgments

The authors thank Gwendoline Tommi-Morin, Antoine Biehler, Marie-Pier Tremblay, and Frederike Lemay-Borduas for valuable field assistance; Marie-André Roy for producing Fig. 1; Katheryn Balind for technical laboratory assistance with EA-IRMS; and Laure Devine for English revisions. The authors also acknowledge the participation of Claude and Kathia Bourque for allowing access to their beach and for their welcome. Two anonymous referees are gratefully acknowledged for their constructive comments on the original manuscript. This research was supported by the Canada Research Chair Program, grants from the Natural Sciences and Engineering Research Council of Canada to Gwénaëlle Chaillou, and the Université du Québec à

Rimouski. Partial funding was provided by Fonds de recherche du Québec Nature et Technologies, UQAR, and Québec-Océan to Maude Sirois.

Table 1: Mean δ^{13}C-DOC signatures (‰) and DOC concentrations (mM) for the different potential sources of DOC (fresh inland groundwater and seawater).

Figure 1: (a) Province of Quebec, (b) the Îles-de-la-Madeleine, and (c) the archipelago's main island (Cap-aux-Meules). The study area of Martinique Beach and the wells where fresh inland groundwater was collected are shown in panel C. The simplified geology was adapted from Brisebois (1981).

Figure 2: Cross-shore transect on the studied beach in 2013 (grey) and 2015 (black). A) Locations of the different multi-level samplers (M1 to M9). The sampling points are also reported (grey squares for 2013 and black circles for 2015). B) Location of the different sampling points for sediment. The beach morphology was obtained from differential global positioning system (DGPS) measurements. The indicated depths are relative to mean sea level (i.e., 0 m=sea level). C) Photography of the studied beach in 2013 and D) in 2015 with the seaweed deposits.

Figure 3: Cross-sections of transect of M1 to M9 showing the topography and distribution of salinity (A, B, C), total dissolved Fe concentrations (D, E, F), DOC concentrations (G, H, I), and δ^{13}C-DOC (J, K, L) for the three sampling campaigns. Contour lines were determined by spatial interpolation (kriging method). Black dots represent each sampling point. Depths are relative to mean sea level (0 m=sea level).

Figure 4: Percent OC (top panels) and δ^{13}C-POC (bottom panels) of each sediment core in 2013 (C1, C3, and C4) and 2015 (C2 and C5). Results are given for each sedimentary unit (C = Holocene sand; P = organic-rich horizon; S = Permian sandstone). The locations of the different sedimentary cores are reported in Fig. 2B. The sedimentary unit P is absent at the low-tide mark which explains why there is no result for C4 and C5 for this unit.

Figure 5: Percent total OC associated with Fe (top panels) and δ^{13}C-POC of the OC associated with Fe for each sediment core (bottom panels) in 2013 (C1, C3, and C4) and 2015 (C2 and C5). Results are given for each sedimentary unit (C = Holocene sand; P = organic-rich layer horizon; S = Permian sandstone). The locations of the different sedimentary cores are reported in Fig. 2B. The sedimentary unit P is absent at the low-tide mark, which explains why there is no result for C4 and C5 for this unit.

Figure 6: Relationship between δ^{13}C-DOC (‰) and DOC concentration (mM). The black dots represent the values measured in 2013, while the dark gray dots represent the 2015-A values and the light gray dots represent the 2015-B values.

References

Anschutz, P., Smith, T., Mouret, A., Deborde, J., Bujan, S., Poirier, D., Lecroart, P., 2009. Tidal sands as biogeochemical reactors. Estuar. Coast. Shelf Sci. 84, 84–90. doi:10.1016/j.ecss.2009.06.015

Aravena, R., Wassenaar, L.I., 1993. Dissolved organic carbon and methane in a regional confined aquifer, Southern Ontario, Canada : carbon isotope evidence for associated subsurface sources. Appl. Geochem. 8, 483–493. doi:10.1016/0883-2927(93)90077-T

Aravena, R., Wassenaar, L.I., Spiker, E.C., 2004. Chemical and carbon isotopic composition of dissolved organic carbon in a regional confined methanogenic aquifer. Isotopes Environ. Health Stud. 40, 103–14. doi:10.1080/10256010410001671050

Barber, A., Brandes, J., Leri, A., Lalonde, K., Balind, K., Wirick, S., Wang, J., Gélinas, Y., 2017a. Preservation of organic matter in marine sediments by inner-sphere interactions with reactive iron. Sci. Rep. 7, 366. doi:10.1038/s41598-017-00494-0

Barber, A., Sirois, M., Chaillou, G., Gélinas, Y., 2017b. Stable isotope analysis of dissolved organic carbon in Canada's eastern coastal waters. Limnol. Oceanogr., in press doi:10.1002/lno.10666

Barnett, R.L., Bernatchez, P., Garneau, M., Juneau, M.N., 2017. Reconstructing late holocene relative sea-level changes at the Magdalen Islands (Gulf of St. Lawrence, Canada) using multi-proxy analyses. J. Quat. Sci. 32, 380-395.

Bauer, J.E., Cai, W.-J., Raymond, P. A., Bianchi, T.S., Hopkinson, C.S., Regnier, P.A.G., 2013. The changing carbon cycle of the coastal ocean. Nature 504, 61–70. doi:10.1038/nature12857

Beck, A.J., Tsukamoto, Y., Tovar-Sanchez, A., Huerta-Diaz, M., Bokuniewicz, H.J., Sañudo-Wilhelmy, S.A., 2007. Importance of geochemical transformations in determining submarine groundwater discharge-derived trace metal and nutrient fluxes. Appl. Geochemistry 22, 477–490. doi:10.1016/j.apgeochem.2006.10.005

Beck, M., Reckhardt, A., Amelsberg, J., Bartholomä, A., Brumsack, H.J., Cypionka, H., Dittmar,

T., Engelen, B., Greskowiak, J., Hillebrand, H., Holtappels, M., Neuholz, R., Köster, J., Kuypers, M.M.M., Massmann, G., Meier, D., Niggemann, J., Paffrath, R., Pahnke, K., Rovo, S., Striebel, M., Vandieken, V., Wehrmann, A., Zielinski, O., 2017. The drivers of biogeochemistry in beach ecosystems: A cross-shore transect from the dunes to the low-water line. Mar. Chem. 190, 35–50. doi:10.1016/j.marchem.2017.01.001

Bianchi, T.S., 2011. The role of terrestrially derived organic carbon in the coastal ocean: A changing paradigm and the priming effect. Proc. Natl. Acad. Sci. 108, 19473–19481. doi:10.1073/pnas.1017982108

Bouillon, S., Yambélé, A., Spencer, R.G.M., Gillikin, D.P., Hernes, P.J., Six, J., Merckx, R., Borges, A.V., 2012. Organic matter sources, fluxes and greenhouse gas exchange in the Oubangui River (Congo River basin). Biogeosciences 9, 2045–2062. doi:10.5194/bg-9-2045-2012

Boyle, E.A., Edmond, J.M., Sholkovitz, E.R., 1977. The mechanism of iron removal in estuaries. Geochim. Cosmochim. Acta 41, 1313–1324. doi:10.1016/0016-7037(77)90075-8

Brisebois, D., 1981. Lithostratigraphie des strates permo carbonifères de l'archipel des Îles-de-la-Madeleine. Ministère de l'Énergie et des Ressources Direction Générale des Energies Conventionnelles, Service de l'Exploration, Québec, Canada, Rep. DPV-796.

Chaillou, G., Couturier, M., Tommi-Morin, G., Rao, A.M., 2014. Total alkalinity and dissolved inorganic carbon production in groundwaters discharging through a sandy beach. Procedia Earth Planet. Sci. 10, 88–99. doi:10.1016/j.proeps.2014.08.017

Chaillou, G., Lemay-Borduas, F., Couturier, M., 2016. Transport and transformations of groundwater-borne carbon discharging through a sandy beach to coastal ocean. Can. Water Resour. J. 38, 809–828. doi:10.1080/07011784.2015.1111775

Chaillou, G., Lemay-Borduas, F., Larocque, M., Biehler, A., Tommi-Morin, G., 2018. Flow and discharge of groundwater from a snowmelt-affeced sandy beach. J. Hydrol. 57, 4-15.

Charbonnier, C., Anschutz, P., Poirier, D., Bujan, S., Lecroart, P., 2013. Aerobic respiration in a high-energy sandy beach. Mar. Chem. 155, 10–21. doi:10.1016/j.marchem.2013.05.003

Charette, M.A., Sholkovitz, E.R., 2006. Trace element cycling in a subterranean estuary: Part 2. Geochemistry of the pore water. Geochim. Cosmochim. Acta 70, 811–826. doi:10.1016/j.gca.2005.10.019

Charette, M.A., Sholkovitz, E.R., 2002. Oxidative precipitation of groundwater-derived ferrous iron in the subterranean estuary of a coastal bay. Geophys. Res. Lett. 29, 1–4. doi:10.1029/2001GL014512

Charette, M.A., Sholkovitz, E.R., Hansel, C.M., 2005. Trace element cycling in a subterranean estuary: Part 1. Geochemistry of the permeable sediments. Geochim. Cosmochim. Acta 69, 2095–2109. doi:10.1016/j.gca.2004.10.024

Chmura, G.L., Aharon, P., 1995. Stable carbon isotope signatures of sedimentary carbon in coastal wetlands as indicators of salinity regime. J. Coast. Res. 11, 124–135.

Couturier, M., Nozais, C., Chaillou, G., 2016. Microtidal subterranean estuaries as a source of fresh terrestrial dissolved organic matter to the coastal ocean. Mar. Chem. 186, 46–57. doi:10.1016/j.marchem.2016.08.001

Couturier, M., Tommi-Morin, G., Sirois, M., Rao, A., Nozais, C., Chaillou, G., 2017. Nitrogen transformations along a shallow subterranean estuary. Biogeosciences 14, 3321–3336. doi:10.5194/bg-2016-535

Dorsett, A., Cherrier, J., Martin, J.B., Cable, J.E., 2011. Assessing hydrologic and biogeochemical controls on pore-water dissolved inorganic carbon cycling in a subterranean estuary: A ^{14}C and ^{13}C mass balance approach. Mar. Chem. 127, 76–89. doi:10.1016/j.marchem.2011.07.007

Edzwald, J.K., Upchurch, J.B., O'Melia, C.R., 1974. Coagulation in estuaries. Environ. Sci. Technol. 8, 58–63. doi:10.1021/es60086a003

Emery, K., 1968. Relict sediments on continental shelves of the world. Am. Assoc. Pet. Geol. Bull. 52, 445–464.

Filip, Z., Smed-Hildmann, R., 1992. Does fossil plant material release humic substances into groundwaters? Sci. Total Environ. 117, 313–317. doi:10.1016/0048-9697(92)90098-D

Goñi, M.A., Gardner, L.R., 2004. Seasonal dynamics in dissolved organic carbon concentrations in a coastal water-table aquifer at the forest-marsh interface. Aquat. Geochemistry 9, 209–232. doi:10.1023/B:AQUA.0000022955.82700.ed

Gregory, J., Duan, J., 2001. Hydrolyzing metal salts as coagulants. Pure Applied Chem. 73, 2017–2026. doi:10.1351/pac200173122017

Guy, R.D., Fogel, M.L., Berry, J.A., 1993. Photosynthetic fractionation of the stable isotopes of oxygen and carbon. Plant Physiol. 101, 37–47. doi:10.1104/pp.101.1.37

Haese, R.R., 2006. The biogeochemistry of iron, 2nd edition., Marine Geochemistry. Springer Verlag, Berlin, Heidelberg. doi:10.1007/3-540-32144-6_7

Hayes, J.M., 1993. Factors controlling ^{13}C contents of sedimentary organic compounds: principles and evidence. Mar. Geol. 113, 111–125. doi:10.1016/0025-3227(93)90153-M

Hedges, J.I., Keil, R.G., 1995. Sedimentary organic matter preservation: an assessment and speculative synthesis. Mar. Chem. 49, 137–139. doi:10.1016/0304-4203(95)00013-H

Hedges, J.I., Keil, R.G., Benner, R., 1997. What happens to terrestrial organic matter in the ocean? Org. Geochem. 27, 195–212. doi:10.1016/S0146-6380(97)00066-1

Hedges, J.I., Stern, J.H., 1984. Carbon and nitrogen determinations of carbonate-containing solids. Limnol. Oceanogr. 29, 657–663. doi:10.4319/lo.1984.29.3.0657

Huettel, M., Ziebis, W., Forster, S., 1996. Flow-induced uptake of particulate matter in permeable sediments. Limnol. Oceanogr. 151, 41–52. doi:10.4319/lo.1996.41.2.0309

Jones, D.L., Edwards, A.C., 1998. Influence of sorption on the biological utilization of two simple carbon substrates. Soil Biol. Biochem. 30, 1895–1902. doi:10.1016/S0038-0717(98)00060-1

Kaiser, K., Guggenberger, G., 2003. Mineral surfaces and soil organic matter. Eur. J. Soil Sci. 54, 219–236. doi:10.1046/j.1365-2389.2003.00544.x

Kaiser, K., Guggenberger, G., 2000. The role of DOM sorption to mineral surfaces in the preservation of organic matter in soils. Org. Geochem. 31, 711–725. doi:10.1016/S0146-

6380(00)00046-2

Kaiser, K., Guggenberger, G., Haumaier, L., 2004. Changes in dissolved lignin-derived phenols, neutral sugars, uronic acids, and amino sugars with depth in forested haplic arenosols and rendzic leptosols. Biogeochemistry 70, 135–151. doi:10.1023/B:BIOG.0000049340.77963.18

Kaiser, K., Guggenberger, G., Zech, W., 2001. Isotopic fractionation of dissolved organic carbon in shallow forest soils as affected by sorption. Eur. J. Soil Sci. 52, 585–597. doi:10.1046/j.1365-2389.2001.00407.x

Keil, R., Montluçon, D., Prahl, F., Hedges, J., 1994. Sorptive preservation of labile organic matter in marine sediments. Nature 370, 549–552. doi:10.1038/370549a0

Kim, J., Kim, G., 2017. Inputs of humic fluorescent dissolved organic matter via submarine groundwater discharge to coastal waters off a volcanic island (Jeju, Korea). Sci. Rep. 7, 1–9. doi:10.1038/s41598-017-08518-5

Kim, T.-H., Waska, H., Kwon, E., Suryaputra, I.G.N., Kim, G., 2012. Production, degradation, and flux of dissolved organic matter in the subterranean estuary of a large tidal flat. Mar. Chem. 142–144, 1–10. doi:10.1016/j.marchem.2012.08.002

Kim, T.H., Kwon, E., Kim, I., Lee, S.A., Kim, G., 2013. Dissolved organic matter in the subterranean estuary of a volcanic island, Jeju: Importance of dissolved organic nitrogen fluxes to the ocean. J. Sea Res. 78, 18–24. doi:10.1016/j.seares.2012.12.009

Kim, J. and G., Kim, 2017. Inputs of humic fluorescent dissolved organic matter via submarine groundwater discharge to coastal waters off a volcanic island (Jeju, Korea). Scientific Reports 7: 7921. doi:10.1038/s41598-017-08518-5

Lalonde, K., Middlestead, P., Gélinas, Y., 2014a. Automation of $^{13}C/^{12}C$ ratio measurement for freshwater and seawater DOC using high temperature combustion. Limnol. Oceanogr. Methods 12, 816–829. doi:10.4319/lom.2014.12.816

Lalonde, K., Mucci, A., Ouellet, A., Gélinas, Y., 2012. Preservation of organic matter in sediments promoted by iron. Nature 483, 198–200. doi:10.1038/nature10855

Lalonde, K., Vähätalo, A.V., Gélinas, Y., 2014b. Revisiting the disappearance of terrestrial dissolved organic matter in the ocean: A $\delta^{13}C$ study. Biogeosciences 11, 3707–3719. doi:10.5194/bg-11-3707-2014

Linkhorst, A., Dittmar, T., Waska, H., 2017. Molecular fractionation of dissolved organic matter in a shallow subterranean estuary: the role of the iron curtain. Environ. Sci. Technol. 51, 1312–1320. doi:10.1021/acs.est.6b03608.

Madelin'Eau. 2004. Gestion des eaux souterraines aux Îles-de-la-Madeleine un défi de développement durable rapport final. 58 p.

Maher, D.T., Santos, I.R., Golsby-Smith, L., Gleeson, J., Eyre, B.D., 2013. Groundwater-derived dissolved inorganic and organic carbon exports from a mangrove tidal creek: The missing mangrove carbon sink? Limnol. Oceanogr. 58, 475–488. doi:10.4319/lo.2013.58.2.0475

McLachlan, A., Brown, A.C., 2006. The ecology of sandy shores, Academic P. ed. Burlington, MA.

Mehra, O.P., Jackson, M.L., 1960. Iron oxide removal from soils and clays by a dithionite-citrate system buffered with sodium bicarbonate. Clays anf Clay Miner. 7, 317–327.

Moore, W.S., 1999. The subterranean estuary: A reaction zone of ground water and sea water. Mar. Chem. 65, 111–125. doi:10.1016/S0304-4203(99)00014-6

Nevin, K.P., Lovley, D.R., 2002. Mechanisms for Fe(III) oxide reduction in sedimentary environments. Geomicrobiol. J. 19, 141–159. doi:10.1080/01490450252864253

Osburn, C.L., Stedmon, C.A., 2011. Linking the chemical and optical properties of dissolved organic matter in the Baltic-North Sea transition zone to differentiate three allochthonous inputs. Mar. Chem. 126, 281–294. doi:10.1016/j.marchem.2011.06.007

Palmer, S.M., Hope, D., Billett, M.F., Dawson, J.J.C., Bryant, C.L., 2011. Sources of organic and inorganic carbon in a headwater stream: evidence from carbon isotope studies. Biogeochemistry 52, 321–338. doi:10.1023/A:1006447706565

Peterson, B.J., Fry, B., 1987. Stable isotopes in ecosystem studies. Annu. Rev. Ecol. Syst. 293–

320. doi:10.1146/annurev.es.18.110187.001453

Poulin, B.A., Ryan, J.N., Aiken, G.R., 2014. The effects of iron on optical properties of dissolved organic matter. Environ. Sci. Technol. 48, 10098–10106. doi:10.1021/es502670r

Raymond, P.A., Bauer, J.E., 2001. Use of ^{14}C and ^{13}C natural abundances for evaluating riverine, estuarine, and coastal DOC and POC sources and cycling: A review and synthesis. Org. Geochem. 32, 469–485. doi:10.1016/S0146-6380(00)00190-X

Riedel, T., Biester, H., Dittmar, T., 2012. Molecular fractionation of dissolved organic matter with metal salts. Environ. Sci. Technol. 46, 4419–4426. doi:10.1021/es203901u

Riedel, T., Zak, D., Biester, H., Dittmar, T., 2013. Iron traps terrestrially derived dissolved organic matter at redox interfaces. Proc. Natl. Acad. Sci. 110, 10101–10105. doi:10.1073/pnas.1221487110

Roy, M., Martin, J.B., Cable, J.E., Smith, C.G., 2013. Variations of iron flux and organic carbon remineralization in a subterranean estuary caused by inter-annual variations in recharge. Geochim. Cosmochim. Acta 103, 301–315. doi:10.1016/j.gca.2012.10.055

Sanderman, J., Lohse, K.A., Baldock, J.A., Amundson, R., 2009. Linking soils and streams: Sources and chemistry of dissolved organic matter in a small coastal watershed. Water Resour. Res. 45, 1–13. doi:10.1029/2008WR006977

Sanders, C.J., Santos, I.R., Sadat-Noori, M., Maher, D.T., Holloway, C., Schnetger, B., 2017. Uranium export from a sandy beach subterranean estuary in Australia. Estuar. Coast. Shelf Sci. 1–33. doi:10.1016/j.ecss.2017.09.002

Santos, I.R., Burnett, W.C., Chanton, J., Mwashote, B., Suryaputra, I.G.N.A., Dittmar, T., 2008. Nutrient biogeochemistry in a Gulf of Mexico subterranean estuary and groundwater-derived fluxes to the coastal ocean. Limnol. Oceanogr. 53, 705–718. doi:10.4319/lo.2008.53.2.0705

Santos, I.R., Burnett, W.C., Dittmar, T., Suryaputra, I.G.N.A, Chanton, J., 2009. Tidal pumping drives nutrient and dissolved organic matter dynamics in a Gulf of Mexico subterranean estuary. Geochim. Cosmochim. Acta 73, 1325–1339. doi:10.1016/j.gca.2008.11.029

Seidel, M., Beck, M., Greskowiak, J., Riedel, T., Waska, H., Suryaputra, I.G.N.A., Schnetger, B., Niggemann, J., Simon, M., Dittmar, T., 2015. Benthic-pelagic coupling of nutrients and dissolved organic matter composition in an intertidal sandy beach. Mar. Chem. 176, 150–163. doi:10.1016/j.marchem.2015.08.011

Seidel, M., Beck, M., Riedel, T., Waska, H., Suryaputra, I.G.N.A., Schnetger, B., Niggemann, J., Simon, M., Dittmar, T., 2014. Biogeochemistry of dissolved organic matter in an anoxic intertidal creek bank. Geochim. Cosmochim. Acta 140, 418–434. doi:10.1016/j.gca.2014.05.038

Shen, Y., Chapelle, F.H., Strom, E.W., Benner, R., 2015. Origins and bioavailability of dissolved organic matter in groundwater. Biogeochemistry 122, 61–78. doi:10.1007/s10533-014-0029-4

Shields, M.R., Bianchi, T.S., Gélinas, Y., Allison, M.A., Twilley, R.R., 2016. Enhanced terrestrial carbon preservation promoted by reactive iron in deltaic sediments. Geophys. Res. Lett. 1–25. doi:10.1002/2015GL067388

Sholkovitz, E.R., 1976. Flocculation of dissolved organic and inorganic matter during the mixing of river water and seawater. Geochim. Cosmochim. Acta 40, 831–845. doi:10.1016/0016-7037(76)90035-1

Wada, S., Aoki, M.N., Tsuchiya, Y., Sato, T., Shinagawa, H., Hama, T., 2007. Quantitative and qualitative analyses of dissolved organic matter released from Ecklonia cava Kjellman, in Oura Bay, Shimoda, Izu Peninsula, Japan. J. Exp. Mar. Bio. Ecol. 349, 344–358. doi:10.1016/j.jembe.2007.05.024

Wagai, R., Mayer, L.M., 2007. Sorptive stabilization of organic matter in soils by hydrous iron oxides. Geochim. Cosmochim. Acta 71, 25–35. doi:10.1016/j.gca.2006.08.047

Weishaar, J., Aiken, G., Bergamaschi, B., Fram, M., Fujii, R., Mopper, K., 2003. Evaluation of specific ultra-violet absorbance as an indicator of the chemical content of dissolved organic carbon. Environ. Sci. Technol. 37, 4702–4708. doi:10.1021/es030360x

Wurl, O., Tsai, M., 2009. In: Wurl,O. (Ed.). Analysis of dissolved and particulate organic carbon

with the HTCO Technique.

Qi, L., Xie, H., Gagné, J.-P., Chaillou, G., Massicotte, P., Yang, G., under review. Photoreactivity of two distinct DOM pools in groundwater of a subarctic island. Mar. Chem.

Yamashita, Y., McCallister, S.L., Koch, B.P., Gonsior, M., Jaffé, R., 2015. Dynamics of dissolved organic matter in fjord ecosystems: Contributions of terrestrial dissolved organic matter in the deep layer. Estuar. Coast. Shelf Sci. 159, 37–49. doi:10.1016/j.ecss.2015.03.024

Zeebe, R.E., Wolf-Gladrow, D., 2001. Stable isotope fractionation. CO_2 seawater equilibrium, Kinet. Isot. 141–250.

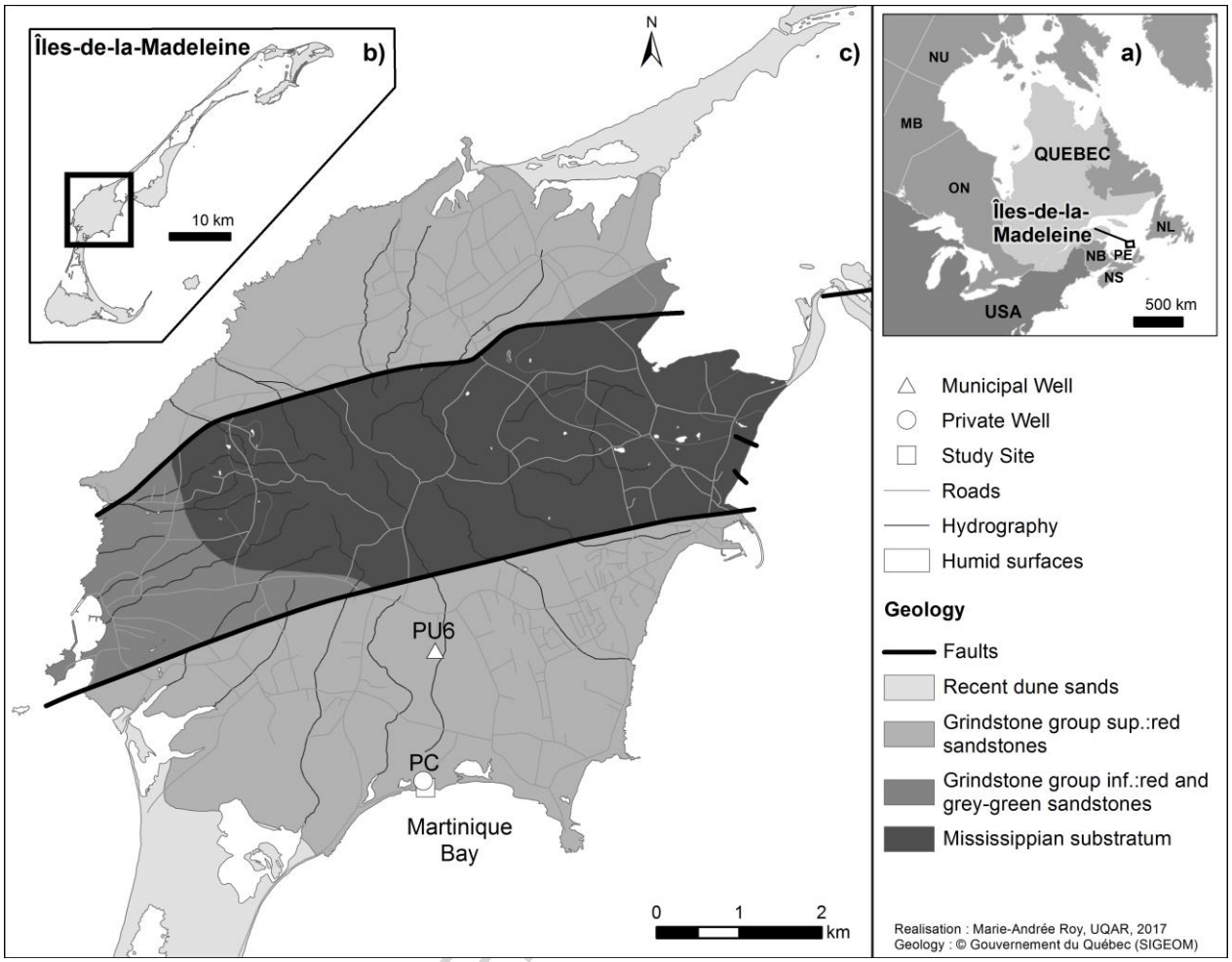

Fig 1

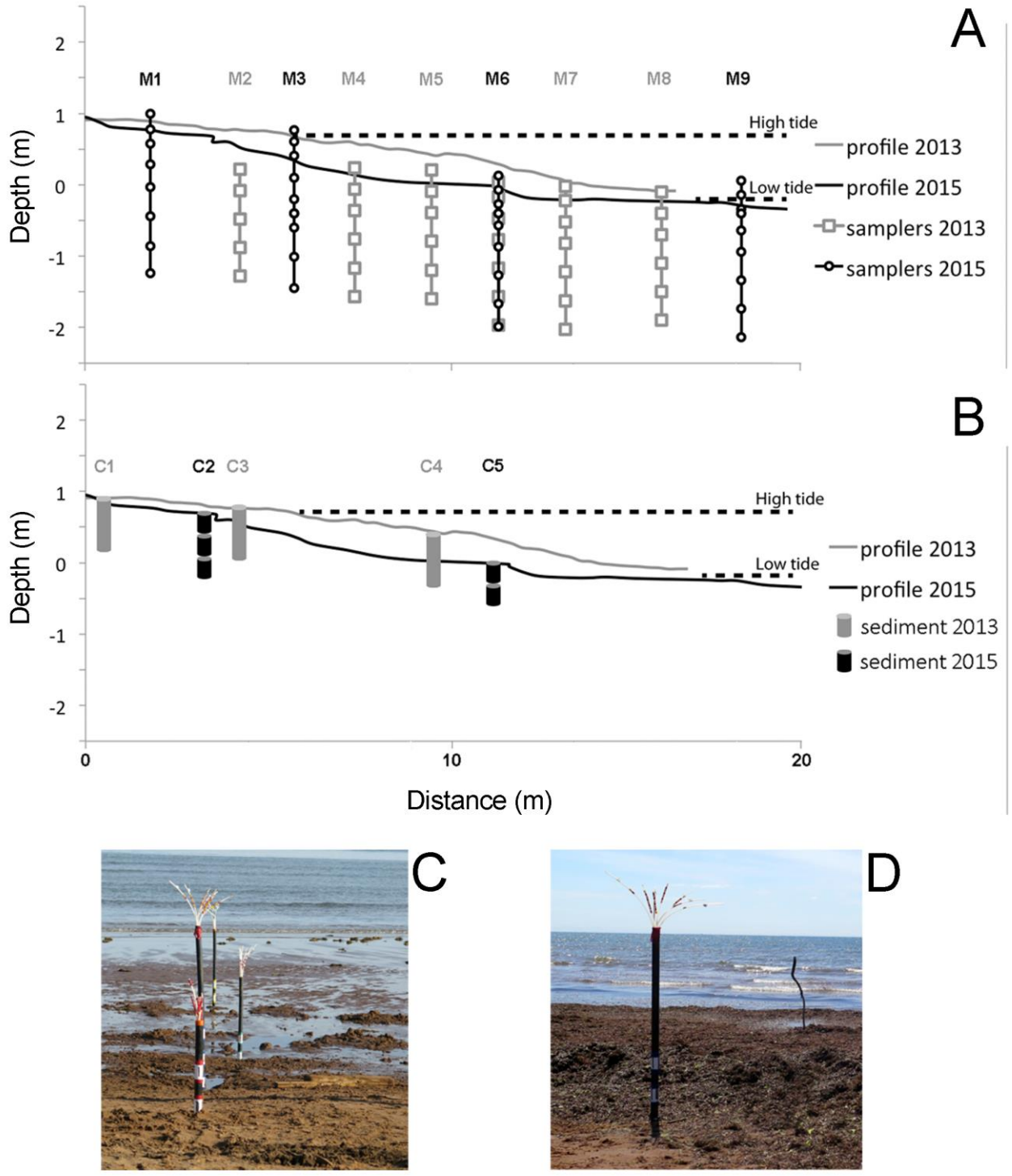

Fig 2

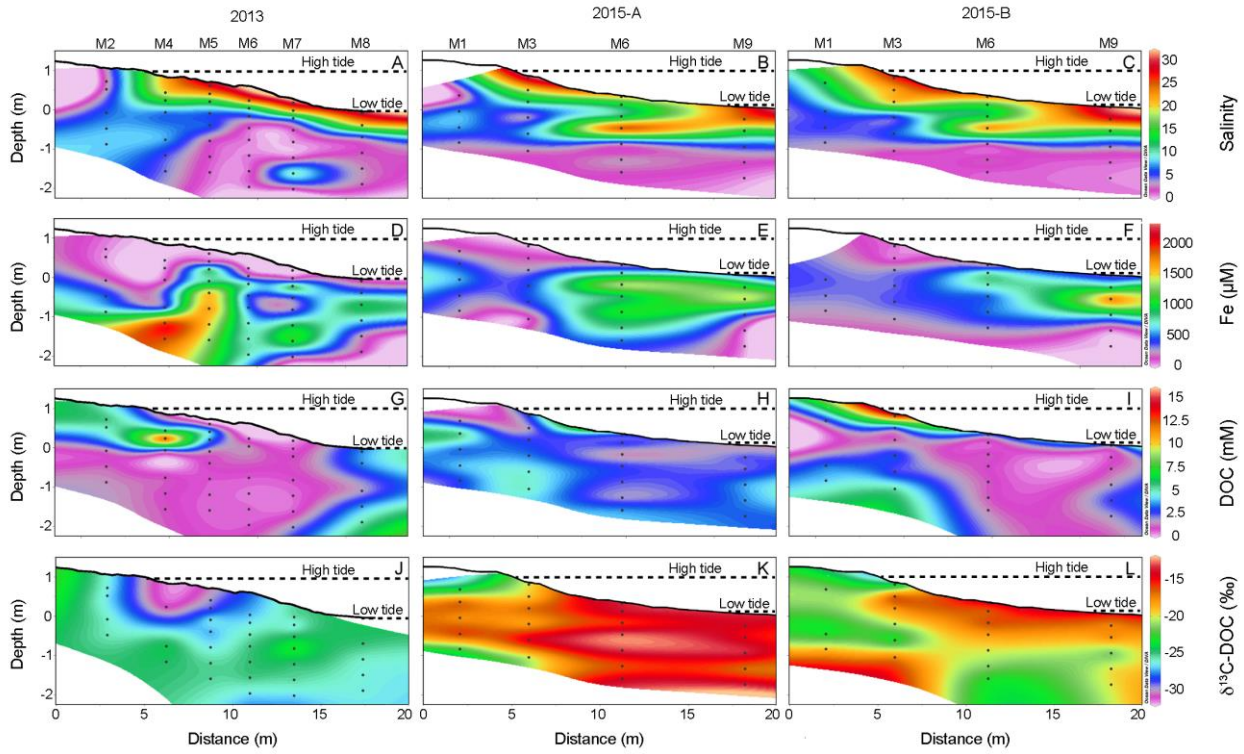

Fig 3

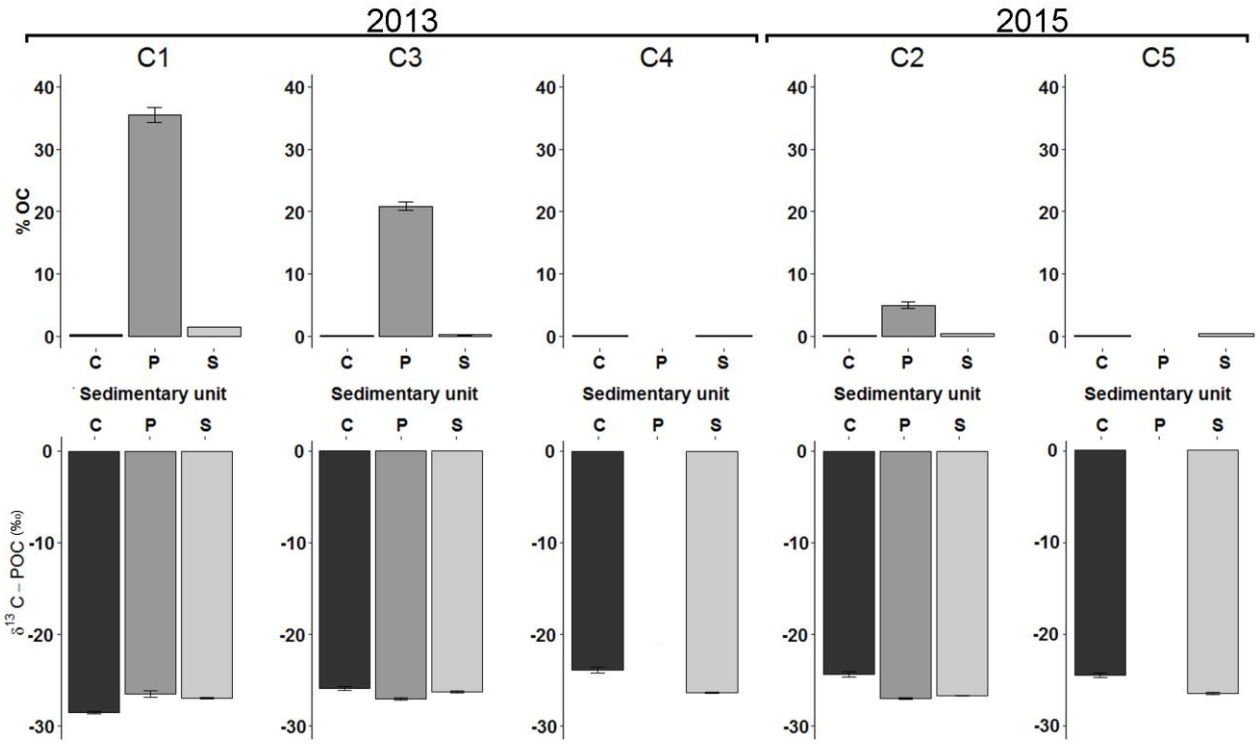

Fig 4

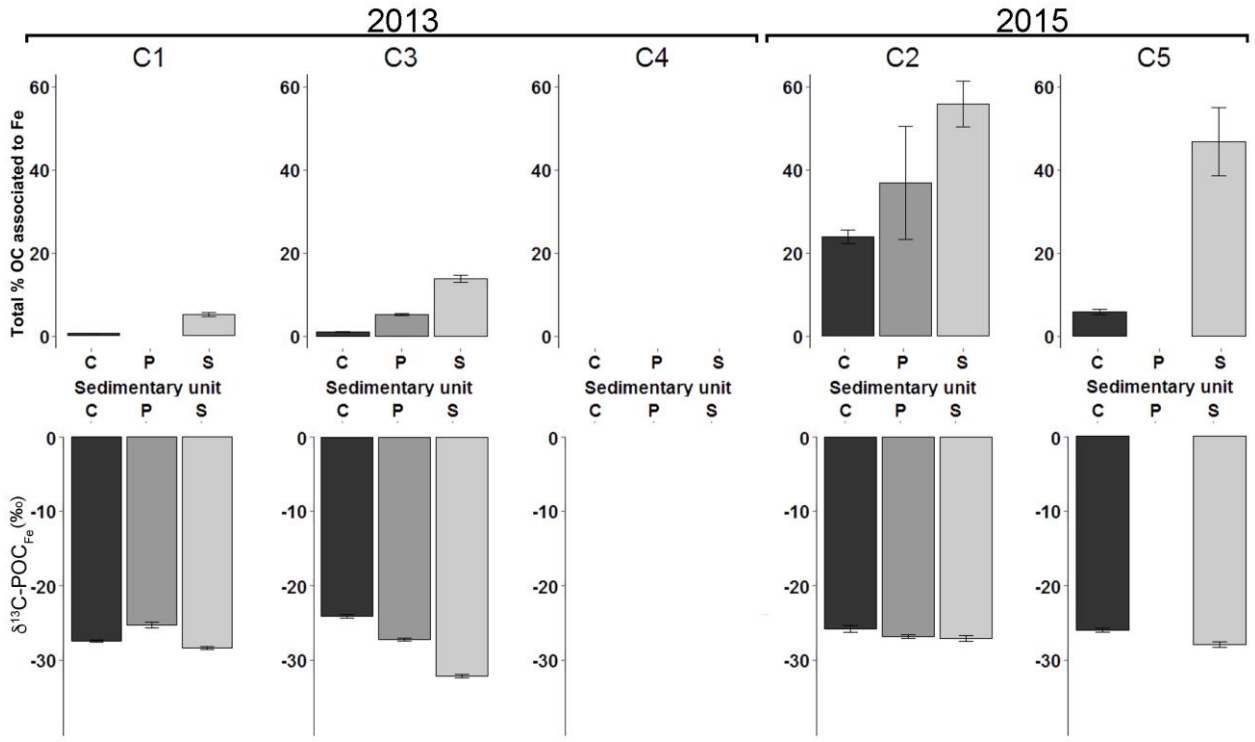

Fig 5

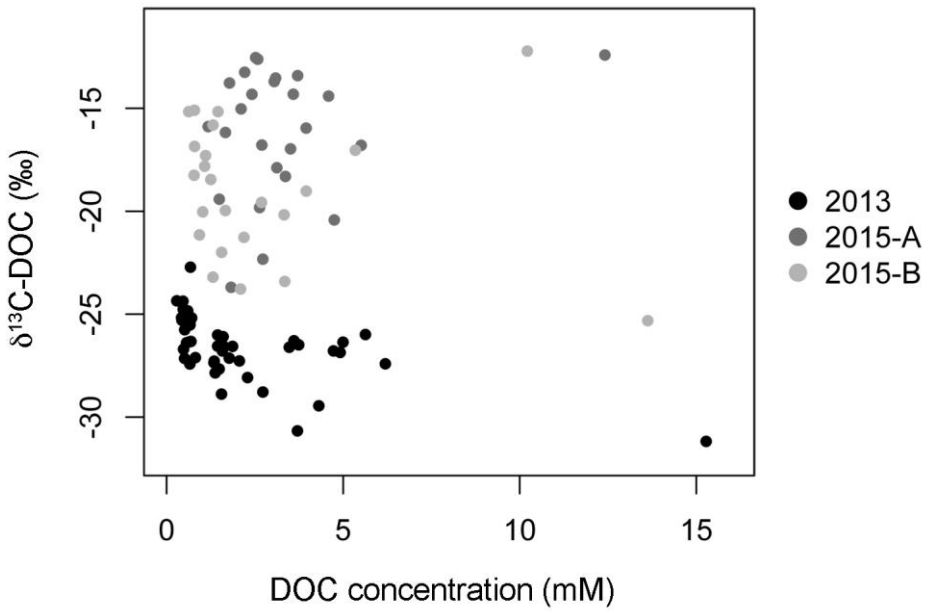

Fig 6

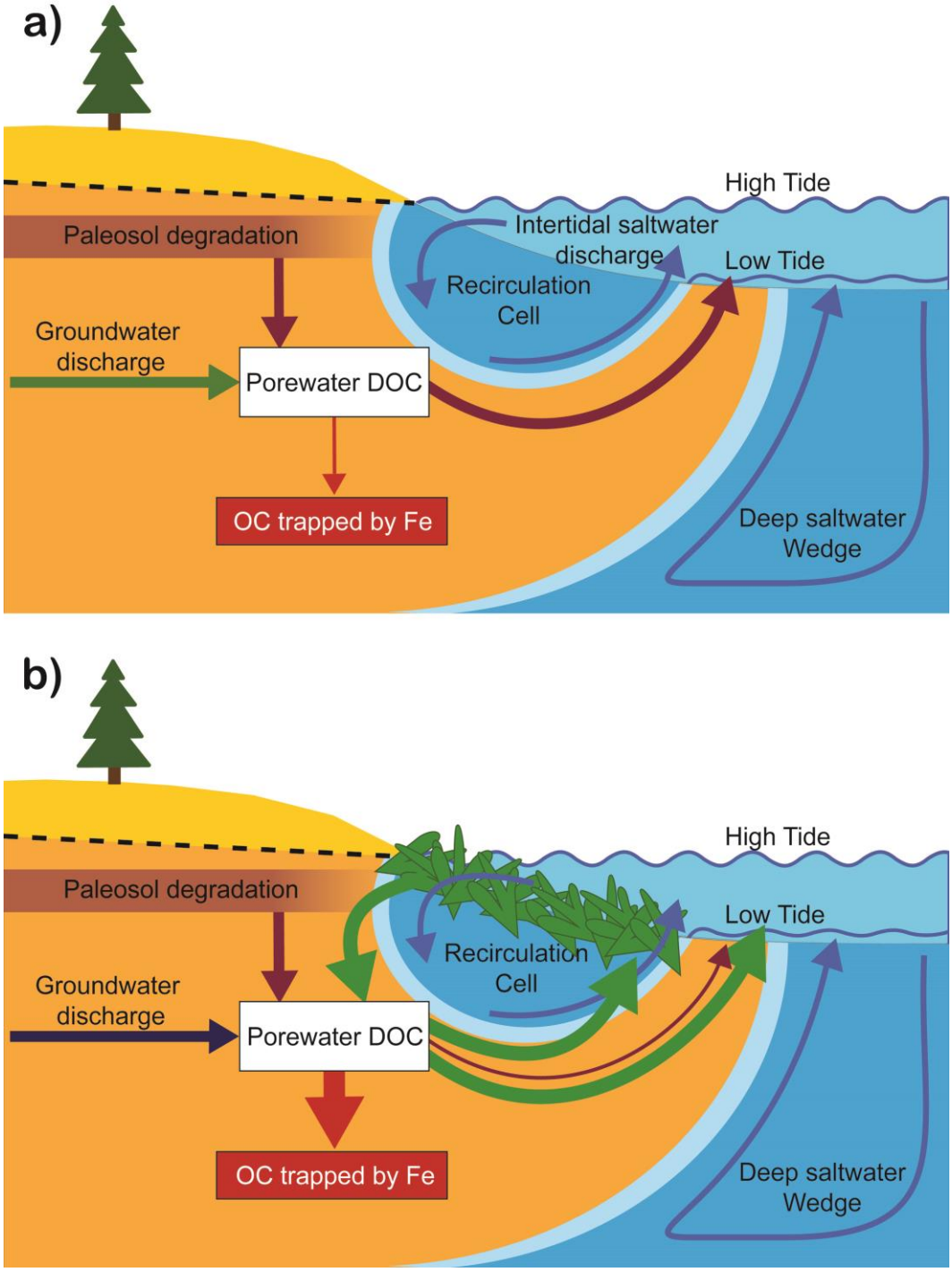

Fig 7

Table 1

Sample	**Source**	δ^{13}**C-DOC (‰)**	**DOC (mM)**
PU6	inland groundwater	-20.6 ± 6.2	0.40 ± 0.18
PC	inland groundwater	-26.0 ± 1.1	2.39 ± 0.45
SW	marine water	-22.1 ± 4.3	0.15 ± 0.02

Highlights

- The δ^{13}C-DOC signal in beach groundwater rapidly responds to OC inputs
- A terrestrial imprint resulting from the POC degradation dominates the δ^{13}C-DOC signature
- Fe-OC trapping occurs in the sandy sediment of the subterranean estuary
- Terrestrial organic carbon was selectively trapped on amorphous Fe-hydroxides
- Sandy beach subterranean estuary acts as a transient sink of terrestrial organic carbon at the land-sea interface